



Arctic Ice Dynamics Joint Experiment (AIDJEX) assumptions revisited and found inadequate

Max Coon,¹ Ron Kwok,² Gad Levy,¹ Matthew Pruis,¹ Howard Schreyer,³ and Deborah Sulsky⁴

Received 14 November 2005; revised 22 February 2007; accepted 21 June 2007; published 14 November 2007.

[1] This paper revisits the Arctic Ice Dynamics Joint Experiment (AIDJEX) assumptions about pack ice behavior with an eye to modeling sea ice dynamics. The AIDJEX assumptions were that (1) enough leads were present in a 100 km by 100 km region to make the ice isotropic on that scale; (2) the ice had no tensile strength; and (3) the ice behavior could be approximated by an isotropic yield surface. These assumptions were made during the development of the AIDJEX model in the 1970s, and are now found inadequate. The assumptions were made in part because of insufficient large-scale (10 km) deformation and stress data, and in part because of computer capability limitations. Upon reviewing deformation and stress data, it is clear that a model including deformation on discontinuities and an anisotropic failure surface with tension would better describe the behavior of pack ice. A model based on these assumptions is needed to represent the deformation and stress in pack ice on scales from 10 to 100 km, and would need to explicitly resolve discontinuities. Such a model would require a different class of metrics to validate discontinuities against observations.

Citation: Coon, M., R. Kwok, G. Levy, M. Pruis, H. Schreyer, and D. Sulsky (2007), Arctic Ice Dynamics Joint Experiment (AIDJEX) assumptions revisited and found inadequate, *J. Geophys. Res.*, 112, C11S90, doi:10.1029/2005JC003393.

1. Introduction

[2] In this paper we describe the Arctic pack ice within the scope of modeling ice dynamics and deformation. The focus is on ice dynamics and deformations since ice motion is responsible for redistributing freshwater in the Arctic, and ice deformation is the mechanical input to the ice thickness distribution. Resolving the thickness distribution has important consequences for simulating the complete atmosphere-ice-ocean system. The boundary condition that represents the coupling between the atmosphere and the ocean needs to be represented accurately in the presence of sea ice if the climate of high latitudes is to be simulated correctly. Present ice models such as AIDJEX [Coon, 1980], Hibler [1980], and Hunke and Dukowicz [1997], have been shown to model ice motion reasonably well, but do not adequately model deformation. Some of this inadequacy is due to insufficiencies in the model assumptions as compared with observations of pack ice behavior.

[3] The assumptions used in the development of the AIDJEX model [Coon, 1980, p.16] were as follows.

[4] 1. “The AIDJEX elastic-plastic constitutive law was developed in an attempt to describe the large-scale (100 km) behavior of sea ice and to resolve events on a timescale of one day. After examining images of Arctic sea ice obtained from both satellite and airborne sensors, it was decided that cracks, ridges, and leads were quite randomly distributed on length scales of 100 km, and it would be possible to represent the behavior by an isotropic model. One can find times when the cracks, ridges, or leads have preferred directions, and at these times the isotropic model will not be as good.”

[5] 2. Pack ice cannot withstand tensile stress.

[6] 3. The comprehensive strength can be determined from the energy in the ridging processes. These assumptions were adopted by Hibler [1980] and by Hunke and Dukowicz [1997] in formulating their ice models, and therefore many sea ice dynamics models being used today are based on the same assumptions.

[7] In this paper we critically review these assumptions and suggest a different view of the dynamics of pack ice based on different assumptions. The new view of the behavior leads to a model that accounts directly for velocity (displacement) discontinuities, which are related to the formation of leads and ridges and cause anisotropic ice strength. We discuss the kinematics of ice with discontinuities and low concentration, and suggest that a different type of metrics needs to be used to validate such situations. We propose and test such metrics. In separate papers, Schreyer *et al.* [2006] develop an elastic-decohesion ice model based on this discontinuous/anisotropic behavior, and

¹NorthWest Research Associates, Redmond, Washington, USA.

²Jet Propulsion Laboratory, Pasadena, California, USA.

³Department of Engineering, University of New Mexico, Albuquerque, New Mexico, USA.

⁴Department of Mathematics and Statistics, University of New Mexico, Albuquerque, New Mexico, USA.

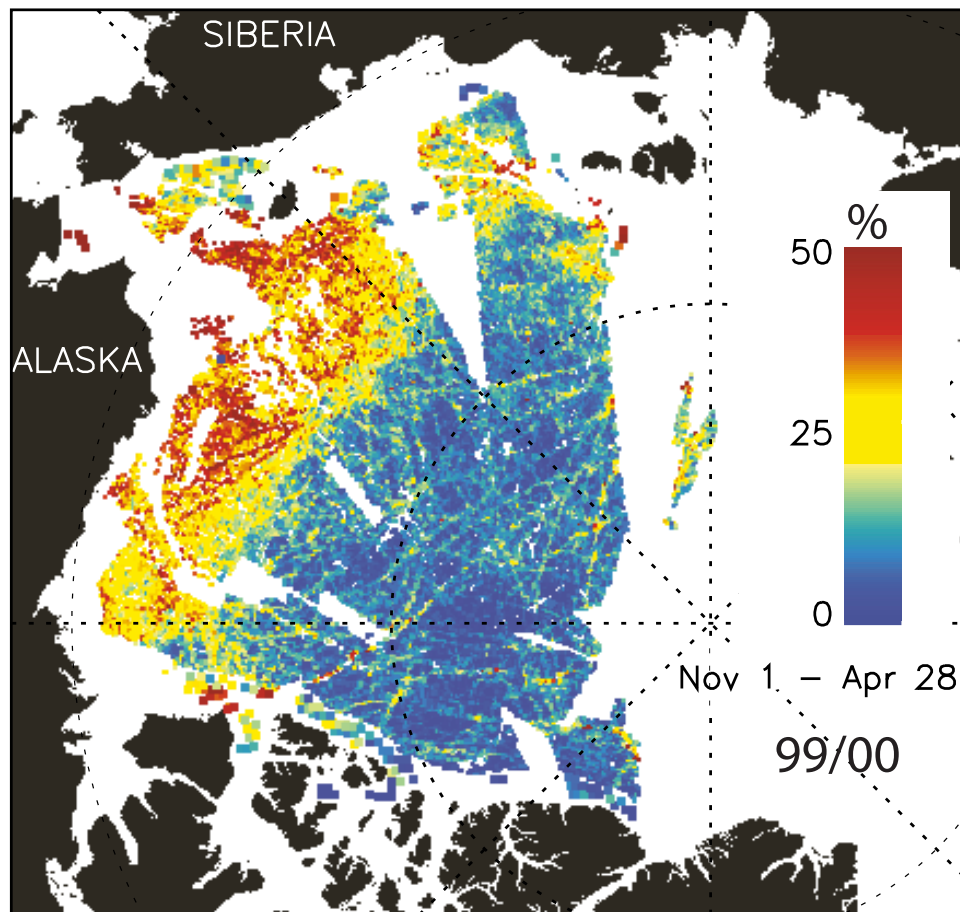


Figure 1. Fractional number of time steps (in percent) a cell is active between 1 November 1999 and 28 April 2000.

Sulsky et al. [2007] describe a method for solving ice dynamic problems with the new model.

2. Deformation and Scales

[8] The first AIDJEX assumption was tested with motion data by *Thorndike and Colony* [1978]. *Thorndike and Colony* [1978] showed, by using AIDJEX position data, that the assumption was not valid. They stated that “the data set considered here from spring and summer 1975 in the Beaufort Sea implies that the true deformation cannot be represented well as constant over lengths of 100 km because it ignores the magnitude of the discontinuities.”

[9] The motion and deformation of the Arctic ice pack can now be determined from buoys and sequential satellite images. Synthetic Aperture Radar (SAR) provides a detailed view of the ice, and when processed using the RADARSAT Geophysical Processor System (RGPS), it provides estimates of sea ice motion and deformation for large regions of the Arctic. The completeness of this data set makes it valuable for describing the important features of Arctic ice dynamics and deformation [e.g., *Kwok*, 2006].

[10] Figure 1 shows the fraction of time a grid cell of sea ice was active over an entire winter. We consider a grid cell active if divergence is greater than 0.02/day or shear is greater than 0.04/day over the data sampling interval. The

most active regions shown occur in first year ice. This is worthy of note since the amount of the ice cover consisting of first year has been observed to be increasing in recent years. Increased activity corresponds to above normal external forcing and/or lower ice strength. The multiyear ice pack shows that large deformation events occur in long-lasting, linear features and correspond to discontinuities in the displacement (or velocity) fields.

[11] Figure 2 shows that the first year ice is most active in the fall, and that first year ice is more active than multiyear ice. This is what one would expect as the ice grows thicker and extends to shore. A striking feature of the RGPS analyses is that most 10 km Lagrangian cells do not have permanent deformation during the year [*Kwok*, 2006].

[12] Figure 3 shows this deformation in a different way by sorting the deformation as a function of space scale for two different fractions of multiyear ice coverage. This figure shows that a only small percent of 10 km cells are active or exhibit deformations that are less than the uncertainties in the RGPS motion estimates. This is more pronounced when a larger percent of the multiyear ice is present. This observation is consistent with the observations of *Marsan et al.* [2004] who show using RADARSAT data that the deformation of sea ice is localized at small scales. Figure 3 also shows that more elements are shearing than opening and closing.

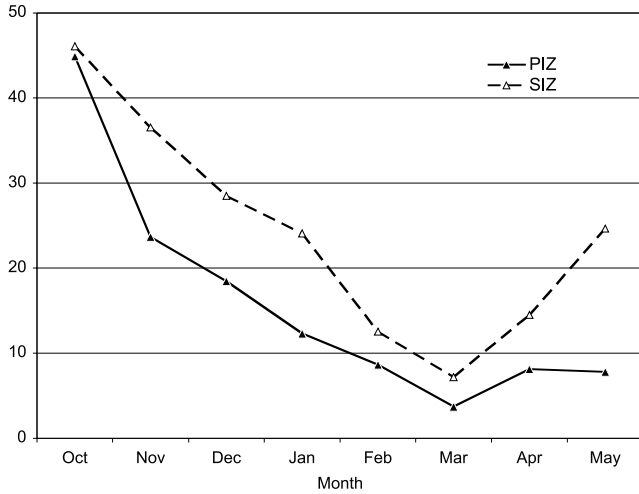


Figure 2. Seasonal change in activity for different ice types. Activity is defined as the fractional number of RGPS cell active in the seasonal ice zone (SIZ) and perennial ice zone (PIZ) during months in 1998/1999 (figure adapted from *Kwok* [2006]). The SIZ consists of first year ice and the PIZ is defined to consist of predominately multiyear ice.

[13] We conclude that thick first year ice and multiyear ice could be approximated with all deformation occurring as discontinuities in the displacement field. It might be possible to increase the element size to be much larger than 100 km in order to satisfy the AIDJEX assumption, but neither the AIDJEX motion data nor the RGPS data products support this. At scales of a few 100 km (this is the size of storms), the air stress forcing will vary substantially over the elements. This view is very different from the AIDJEX assumption, and in the next section we will describe the kinematics of this view.

3. Kinematics of Strong Discontinuities

[14] The RGPS deformation products are based on the assumption that the displacements and velocities are smooth functions of the spatial coordinates. However, if the dominant form of deformation of multiyear ice is in the opening, closing, and shearing of linear features or leads, then the displacements and velocities can be discontinuous. In this section we discuss the kinematics associated with strong discontinuities that describe possible jumps in displacement or velocity.

[15] Consider a region Ω of ice that has a crack surface S dividing the region into Ω^+ and Ω^- , as in Figure 4. The normal n to the surface S points into Ω^+ . A discontinuous displacement field has the form

$$u(x, t) = \bar{u}(x, t) + [[u]]H_S(x). \quad (1)$$

The displacement has been divided into a continuous part \bar{u} and a discontinuous part, where the jump in displacement is $[[u]] = u^+ - u^- = \xi \mathbf{m}$ across the surface S . In general, the jump in displacement varies with position, but for a single RGPS cell, we assume it is independent of x . The magnitude of the jump is ξ and \mathbf{m} is a unit vector giving the jump direction or mode of opening. The function $H_S(x)$ is the

Heaviside function

$$H_S(x) = \begin{cases} 1 & \text{if } x \in \Omega^+ \\ 0 & \text{if } x \in \Omega^- \end{cases}. \quad (2)$$

A (small) strain tensor ε can be computed from equation (1) by taking the symmetric gradient with respect to x ,

$$\varepsilon = (\nabla u)_{sym} = (\nabla \bar{u})_{sym} + ([[u]] \otimes n)_{sym} \delta_S. \quad (3)$$

The function δ_S is the Dirac-delta function on S .

[16] The RGPS data have been analyzed under the assumption that u contains only the continuous part of the displacement field. Strains and strain rates are computed solely from gradients of the displacement or velocity. Suppose we now take an equally extreme view that the observed deformation arises from the discontinuous part of the displacement (or velocity) field. In this case, we wish to find a decohesion strain field, $\varepsilon^d = ([[u]] \otimes n)_{sym} \delta_S$, that best fits the data.

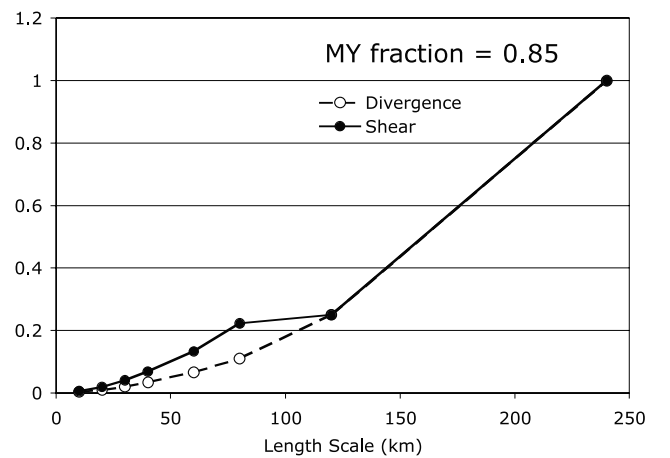
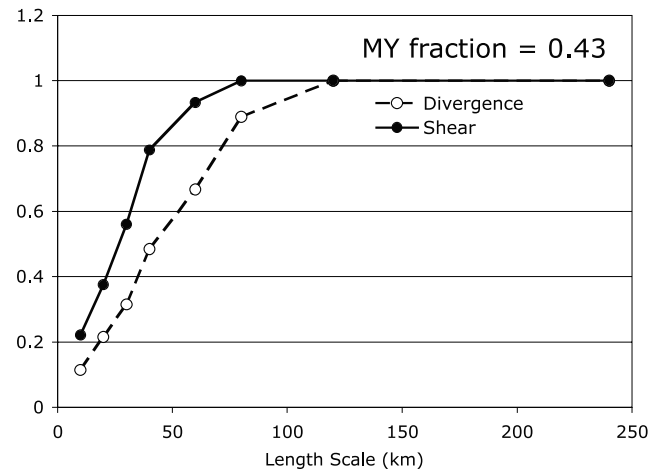


Figure 3. Dependence of activity on spatial length scale under different ice conditions (multiyear ice fraction). Activity is defined as the fractional number of windows at a given length scale with observed divergence or shear over the time period 1–4 February 1999.

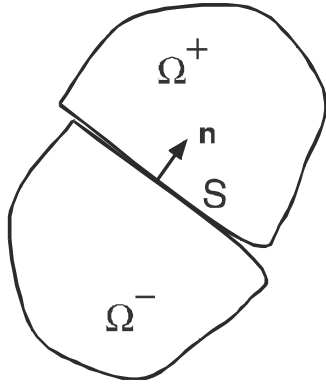


Figure 4. A region of ice Ω that has a crack surface S dividing the region into Ω^+ and Ω^- .

[17] Consider a square element of ice with side length h . Assume the lead goes through the center of this element. Define a rectangular element aligned with a lead with sides of length h_t along the lead direction and h_n normal to the lead, as shown in Figure 5. Specifically,

$$-\pi/4 \leq \theta \leq \pi/4 \quad h_t = h / \cos \theta \quad h_n = h^2 / h_t = h \cos \theta$$

$$\pi/4 \leq \theta \leq 3\pi/4 \quad h_t = h / \sin \theta \quad h_n = h^2 / h_t = h \sin \theta.$$

Thus h_t is the length of the lead and h_n is a perpendicular dimension of a rectangle with the same area, h^2 , as the original element.

[18] We will construct the decohesion strain field by regularizing the delta function distribution over a finite length scale h_n so that the decohesion strain becomes

$$\varepsilon^d = \frac{1}{h_n} ([u] \otimes n)_{sym}. \quad (4)$$

Construct a right-handed nt -coordinate system, where n is the unit normal to the lead and t is tangent to it. In this coordinate system the jump in displacement can be written $[u] = u_n n + u_t t$. Moreover, in the nt -coordinate system, the components of the decohesion strain are

$$\begin{aligned} \varepsilon_{nn}^d &= \frac{u_n}{h_n} \\ \varepsilon_{nt}^d &= \frac{u_t}{2h_n} \\ \varepsilon_{tt}^d &= 0. \end{aligned} \quad (5)$$

When rotated to the original xy -coordinates, the decohesion strains become

$$\begin{aligned} \varepsilon_{xx}^d &= \frac{u_n}{h} \frac{\cos^2 \theta}{\sin \theta} - \frac{u_t}{h} \cos \theta & \varepsilon_{yy}^d &= \frac{u_n}{h} \sin \theta - \frac{u_t}{h} \cos \theta \\ \varepsilon_{xy}^d &= \frac{u_n}{h} \cos \theta - \frac{u_t}{2h} \frac{\cos^2 \theta - \sin^2 \theta}{\sin \theta} \end{aligned} \quad (6)$$

The goal is to determine θ , u_n and u_t to best fit the observations.

[19] One way to accomplish the goal is to compute xy -components of the strain ε_{xx} , ε_{yy} , and ε_{xy} for an element of ice as is usually done for the RGPS products. Now pick θ , u_n and u_t to minimize the Frobenius norm, E , of the difference in strains. Specifically, define

$$E = \frac{\|\varepsilon - \varepsilon^d\|}{\|\varepsilon\|}, \quad (7)$$

where

$$\begin{aligned} \|\varepsilon\| &= [(\varepsilon_{mm})^2 + (\varepsilon_{tt})^2 + 2(\varepsilon_{nt})^2]^{1/2} \\ &= [(\varepsilon_{xx})^2 + (\varepsilon_{yy})^2 + 2(\varepsilon_{xy})^2]^{1/2}. \end{aligned} \quad (8)$$

An analytical solution to this problem is possible using the Mohr-circle representation of the transformation equations for components of a tensor in a plane. In some cases there are two solutions. In these cases, the solution that preserves the sense of rotation is chosen; that is, the vorticity should have the same sign in the nt system as in the xy system.

[20] Figure 6 shows a 50 km by 50 km region of the Arctic that is identified for study on day 136 of 2002. During an 18.5 hour period a large lead opened and sheared. The above technique for determining a representation of the deformation in terms of discontinuities is applied separately to each of the 100 elements in the satellite image, resulting in Figure 7a. Since all deformation is represented by a jump in displacement through the center of the element, all elements have leads. The opening and shearing of the lead is depicted by a gray patch. A patch with a red border is opening, representing the formation of a new lead. A patch with a blue border is closing, representing closing of a preexisting lead.

[21] It is interesting to examine the predominant leads. For this purpose we only plot leads above a minimum threshold size in Figures 7b–7f. That is, we plot a lead if $u_n^2 + u_t^2 > u_o^2$, for different values of u_o . As u_o increases, fewer leads remain in the plot. Notice that the pattern does not vary much for the range $u_o = 200$ m to $u_o = 1200$ m. Thus for this example the dominant leads have a predicted width of 200 m or greater. We quantify the agreement in section 5.2.

4. Strength and Scales

[22] There were two AIDJEX assumptions about the strength of the ice. At the time those assumptions were made there were no field ice stress data to evaluate these

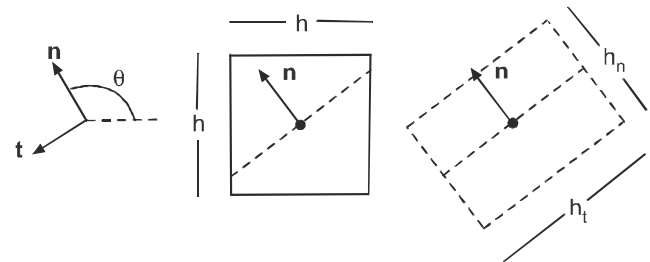


Figure 5. (left) Lead orientation. (middle) Lead goes through center of element and across the element. (right) Lead length is h_t .

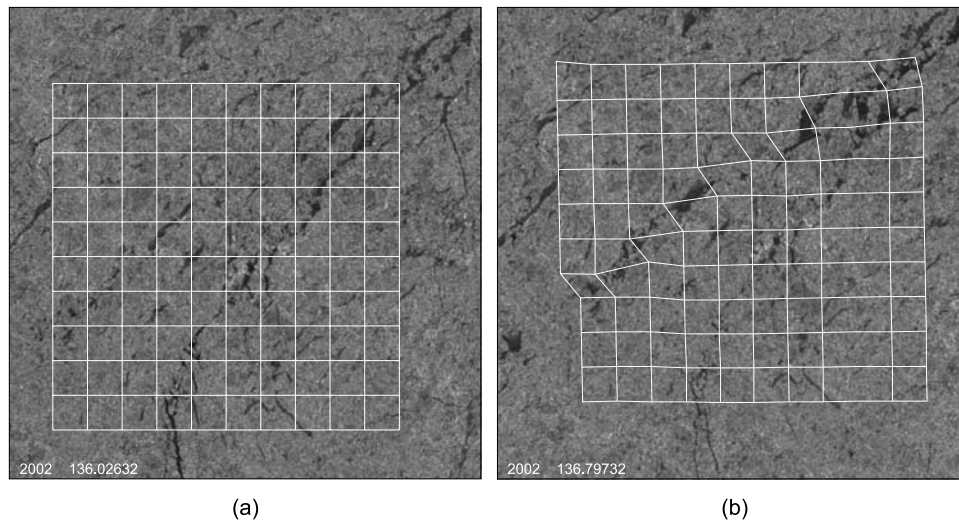


Figure 6. (a) Undeformed and (b) deformed meshes for a 50 km \times 50 km region of the Arctic in May 2002. The deformation occurs over 18.5 hours.

assumptions. In the AIDJEX model the ice was taken to be elastic/plastic, in the Hibler model the ice is viscous/plastic, and in the Hunke model the ice is elastic/viscous/plastic. In all of these models, there is one plastic compressive strength and the tensile strength is zero. In contrast if we accept the view that discontinuities in displacement (velocity) should be accounted for directly, it is clear that the strength parallel to the lead should be different from that perpendicular to it. When a lead is first opened, the stress is normal and shear along the lead would be zero. This view was proposed by *Coon et al.* [1992, 1998a] and *Pritchard* [1998] where the ice is assumed to be plastic. However, in order to model leads directly, the model must be able to find the direction of newly formed leads. The elastic plastic model suggested by *Coon et al.* [1992, 1998a] did not provide the direction of weakening associated with lead formation.

4.1. Isotropic Ice (No Leads)

[23] We now have field ice stress data. If local horizontal stress measurements are indicative of geophysical stress then they should be uniform over a broad region in the central portion of the instrumented ice floe. This was tested by *Coon et al.* [1998b] on a 3 km floe and the stress was shown to be uniform. Therefore the floe was a transducer for measuring large-scale stress.

[24] Ice stress resultant invariant data (for 0.7 m to 1.6 m thick) as reported by *Coon et al.* [1998b] are presented in Figure 8. The data are hourly ice stress measurements plotted as the shear-resultant invariant (half the difference of the principal stress) against the pressure-resultant invariant (average of the principal stress). The data are plotted in search of the envelope corresponding to the failure surface of isotropic ice. The ice stress can have a wide range of values within the envelope when the ice does not fail or where the failure is associated with a preexisting lead or ridge. In a situation where the stress contacts the envelope, isotropic ice fails and forms a slip line or opens a new lead. The data have been sorted by time of the year, and indicate that many of the stress states observed in late winter and early spring are in tension. However, in AIDJEX, it was

assumed that the tensile strength was zero. This was not deduced from measured stress, but from the thinking that if there were many leads in a 100 km element then some would be open at least a little. It is now clear that we do not know how many leads in 100 km or even 10 km are stress free. The data in Figure 8 are from floes 1 to 3 km across. Therefore they may represent the stress resultant on a 10-km scale. Figure 8 also shows yield surfaces for a modified AIDJEX model [*Pritchard*, 1980, 1981] and the *Hibler* [1980] model. The yield surfaces correspond to compact, heavy ice and show little or no tension. Under less compact conditions or in regions with thin ice, the yield surfaces would be smaller. The dimension of the yield surfaces was determined from fitting motion data with model calculations.

[25] The data bring up the question of element scale. In AIDJEX it was taken as 100 km, but many ice dynamic models are now used for much smaller scales (e.g., 10 km). These data indicate that for the smaller scales a much larger yield surface should be used for isotropic-plastic models. These data are in agreement with the finding of *Sanderson* [1988], who examined sea ice strength data from laboratory tests to large-scale field tests. The field data from *Coon et al.* [1998b] are shown to extend the scale of this curve and bridge to the 100-km scale used in ice dynamics models.

4.2. Anisotropic Ice (With Leads)

[26] It is difficult to describe in detail the physical mechanisms for the failure shown in Figure 8. It is clear that new leads result from the failure of isotropic ice. Observation of a lead opening event affords the opportunity to know the regional geophysical ice stress in one direction. While the lead is open, no stress can be transmitted across it; therefore the traction on the lead must be zero.

[27] Such a lead-opening event took place during the SIMI field program [*Coon et al.*, 1998b]. Simultaneous measurements of sea ice stress on both sides of a lead, ice motion from sequential SAR imagery, and ice motion from drifting GPS/Argos buoys were made. The lead, which appeared early in day 35 (4 February) of 1994, was

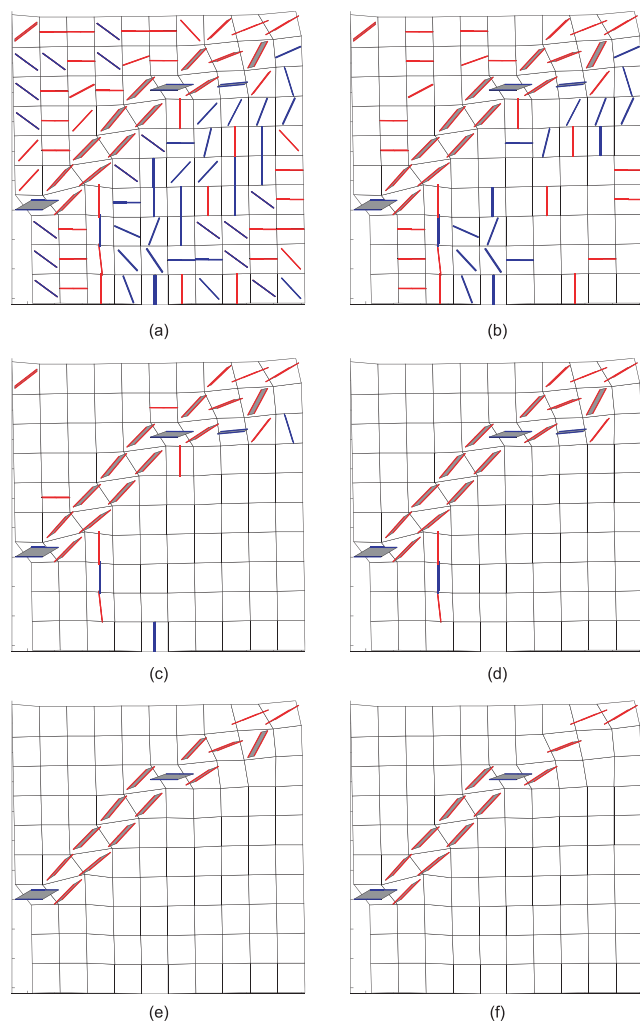


Figure 7. Predicted lead pattern obtained by representing the deformation with a jump in displacement. Red indicates an opening lead and blue indicates the closing of a preexisting lead. Leads are plotted if $u_n^2 + u_t^2 > u_0^2$ where (a) $u_0 = 0$ m, (b) $u_0 = 100$ m, (c) $u_0 = 200$ m, (d) $u_0 = 400$ m, (e) $u_0 = 800$ m, and (f) $u_0 = 1200$ m.

observed, relative motions were calculated across and along the lead direction, and stresses were transformed to this same coordinate system. The lead orientation and approximate location were determined from SAR images of the pack ice surrounding the SIMI camp, as well as from net ice motion at 3-day intervals. The ice motion around the lead was provided in greater temporal detail by an array of drifting GPS/Argos buoys producing hourly positions. Sea-ice stress was measured on each side of the lead.

[28] Figure 9 shows a time series of stress resultant components (for a 2-m-thick floe) in lead coordinates, as calculated from the stress sensor fluid pressures. Near the beginning of day 35, both the shear stress on the lead and the stress normal to the lead direction fell to near zero (and remained near zero for over a week). The principal stress parallel to the lead was variable but remained large.

[29] The stress path in stress-resultant invariant space for hourly data from day 34 to day 40 is shown in Figure 10. As determined from the 6-hourly GPS buoy position data, the

lead is closed at the time marked (A), and is open 6 hours later (marked by point (B) in Figures 9 and 10). A failure surface in invariant space is appropriate for the ice before the lead is open, but after it is open the ice is anisotropic and the failure surface must be expressed by three stress components [Coon *et al.*, 1998a]. Shortly before a lead-opening motion is apparent in the ice motion data, the ice-stress state abruptly changed from biaxial compression to uniaxial compression, with the traction on the lead near zero. This uniaxial behavior of the stress measurements is consistent with the expected geophysical stress during such a lead event.

[30] It is possible to associate these data with a failure surface instead of a plastic yield surface. The difference is that when a stress state reaches the failure surface the pack ice fails as a lead opens. The ice has strength parallel to the lead, but not perpendicular to it. The failure surface of undamaged ice is isotropic, but after the ice fails it is direction dependent (anisotropic). By undamaged ice we mean that any leads or ridges that were active in the element before are now completely healed (refrozen).

[31] Figure 11a shows a representative failure surface for pack ice with no leads. This failure surface is good for all directions in the plane of the pack ice. Figure 11b shows the failure surface for a lead aligned with the σ_2 direction. Figure 11b shows little strength in the σ_1 direction. However, after some ridging or freezing, strength in the σ_1 direction is developed and is indicated in Figure 11c.

4.3. Ridging

[32] The ridging process has been studied with models [Parmeter and Coon, 1972; Hopkins, 1998], laboratory tests [Tuhkuri *et al.*, 1998] and field measurements [Coon and Lau, 1990; Coon *et al.*, 1989]. Bending of the ice is the most important loading in building a pressure ridge. Building the ridge from the ice in a refrozen lead starts with breaking the lead ice. This breaking load may be a larger load than is required to maintain the building process [Hopkins, 1998; Tuhkuri *et al.*, 1998]. As the lead comes together the ridge building force increases, and if the lead is wide enough, the load will reach a limiting height and a corresponding force limit, which are functions of ice thickness. This is expressed by all models and laboratory studies.

[33] Hopkins [1998] developed a simple expression of the limit ridge force in terms of the ice thickness; $F = 95.4h^{1.5}$, where F is the building force kN/m and h is the ice thickness in meters. Using the model of Parmeter and Coon [1972] and ridging forces measured in the field, Coon and Lau [1990] found $F = 113h^{1.5}$. A reasonable approximation of these results therefore might be

$$F = 100h^{1.5}. \quad (9)$$

[34] It is also possible to express the lead width required to reach the ridge height limit, and therefore the load limit, in terms of lead ice thickness. A simplified expression from Parmeter and Coon [1972] is

$$U_L = 1.2 \times \left(\frac{9 \times (0.5 + 0.5t)^2}{t} \right), \quad (10)$$

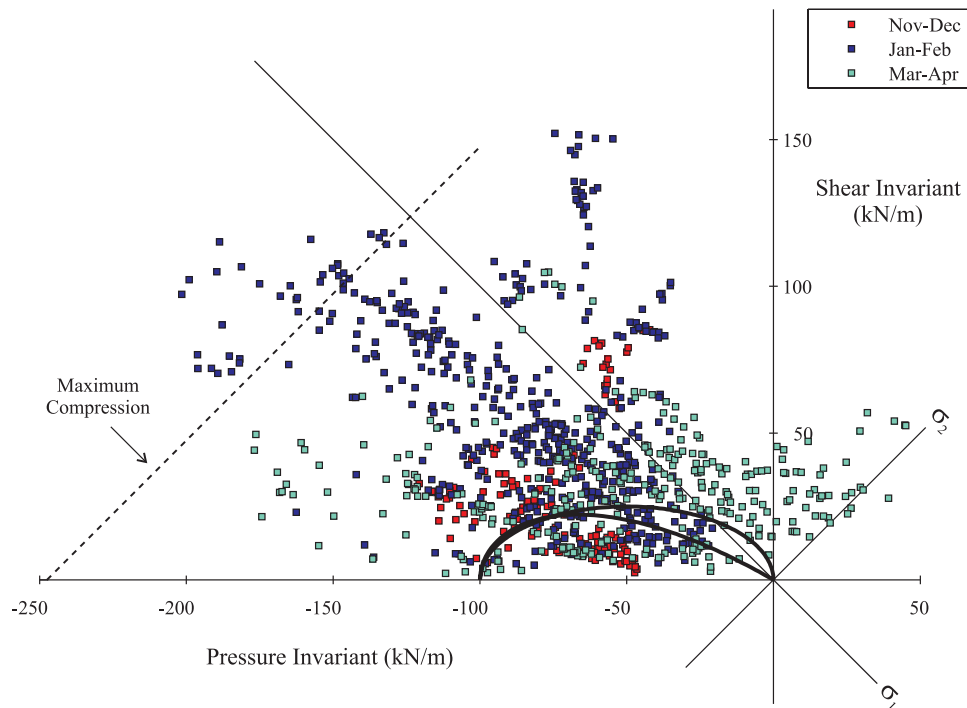


Figure 8. Stress-resultant field data from SIMI sorted by time of year [Coon et al., 1998b]. Also shown is the teardrop yield surface of Pritchard (1980) and the elliptical yield surface of Hibler [1980] adjusted to have the same maximum compressive strength as in work by Pritchard [1980]. Using $P = P^* h \exp(-C(1 - A))$ yields ice thickness, h , of over 3.6 m when the ice coverage, A , is equal to 1 and $P^* = 27.5 \text{ kN/m}^2$ [Hibler, 2004].

where U_L is the lead width for the limit force and t is the lead ice thickness.

[35] In understanding the healing of leads it is helpful to use a simple relation for the growth of ice in the lead such as Lebedev’s parameterization (discussed by Maykut [1986]) using freezing degree days (FDD),

$$t = 0.0133 \times FDD^{0.58}. \tag{11}$$

[36] In Figure 12 the limit ridging force, the lead width required for obtaining the limit force, and the days to grow the ice are plotted against the lead ice thickness. Figure 12 shows that the limit ridging force for 1.4 m ice is the same as the compression force required to fail the isotropic ice shown in Figure 8. A lead width of only about 100 m is required to reach this limit load, but it would take over

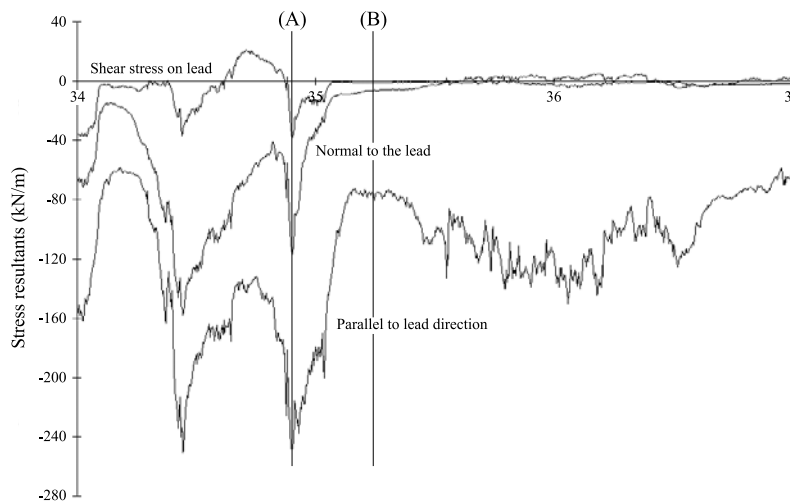


Figure 9. Stress resultant components expressed in label coordinates for a lead opening event during SIMI. Stress measurements made on flow taken to be 2 m thick. Figure modified from Coon et al. [1998a].

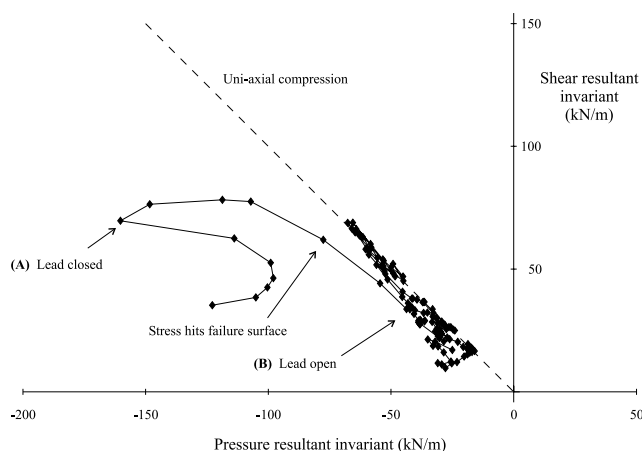


Figure 10. Stress resultant invariants while lead (in Figure 9) was active. Figure modified from *Coon et al.* [1998a].

120 days at -25°C to grow the lead ice to that thickness. Therefore Figure 12 indicates that for most lead ice the limit force will be smaller than the isotropic failure force. This is in agreement with the observations that pressure ridges are made of blocks of thin (i.e., less than 1 m thick) ice. Combining this with the kinematic view above, most 10 km cells will have stress states inside of Figure 11a and the failure surface of Figure 11b will change slowly unless the lead ice is used in ridging.

[37] Sample force displacement curves are sketched in Figure 13. Figure 13a shows the case for a lead with one ice thickness. The limit force is reached at the limit displacement and after some initial break. The limit force continues until the lead is closed and the force becomes that of isotropic ice. Figure 13b shows the case of a lead with two ice thicknesses. When all of the thinnest ice is ridged, the next thinnest ice ridges. In the example shown, however, the ice does not reach its limit force before all of the lead ice is ridged; and the force becomes that of the isotropic ice. These are only two examples of force displacement curves that can be generated. Much of the detail is not needed for an ice dynamic model.

5. Discussion

5.1. Thin, Low Concentration Ice

[38] The mechanical behavior of sea ice is different near the ice edge when compared to the behavior of the central pack ice. The change in behavior is due to the failure (or yield) strength of ice being related to the thickness of the ice and the ice coverage. For example, the long (>100 km), linear velocity discontinuities seen in RGPS data are not present very early in first year ice in the Beaufort and Chukchi Seas. Later during the freezing season, however, these features become visible in RGPS motion data. After a couple of months with air temperatures below -15°C , thermodynamic ice growth (equation (11)) yields an ice thickness of 0.7 m, and the kinematic response of the ice becomes similar to that of multiyear ice. Thermodynamic ice growth is the dominant mechanism in thickening ice, but given the high activity level (e.g., Figure 1) and amount of

total deformation seen in young first-year ice, it is unclear how much thickening of the ice is due to mechanical redistribution.

[39] The dominant factor limiting internal ice stress near the ice edge and in summer is the effect of reduced ice coverage. In the AIDJEX model, it was assumed that there was no internal ice stress in the summer [Coon, 1980]. Hibler [1979] suggested that the failure strength of ice could be related to the ice coverage through an exponential function such that the failure strength is negligible once the ice concentration is around 0.70 (loose packed circular disks give 0.79) and increases to the full failure strength for that ice thickness for an ice concentration of 1. Field data are needed to validate this assumption.

[40] The behavior of thin ice is associated with a smaller isotropic failure surface than would be obtained from Figure 8. Figure 8 shows that 20 kN/m is about 10% of the maximum compressive strength of isotropic ice. From Figure 12 the ridging limit load for 20 kN/m occurs at approximately 0.4 m ice thickness. It appears that the isotropic failure stress for pack ice may go down an order of magnitude for ice thickness from 0.7 to 0.4 m. This does not, however, provide us with the behavior of pack ice with mean thickness of less than 0.7 m. It may be that the behavior can be explained by a discontinuous/anisotropic description with an isotropic failure surface which depends on thickness, or it may be explained with a continuous/isotropic behavior with a yield surface that depends on ice thickness. For thin ice, it may not matter much in the description of ice motion because the internal ice stress term will be small. More field measurements of thin (less than a meter) ice are needed to resolve these issues.

5.2. Metric

[41] The treatment of discontinuities in the displacements (or velocities) of sea ice requires some shift in the procedure for evaluation and validation of models against observations. Grumbine [1998] notes that sea ice literature includes relatively little in the way of quantitative model verification, explaining this by the fact that visual inspection of model output has been sufficiently unambiguous to determine which model or parameterization was better. While this remains the case, a need clearly exists to quantify a model's success and improvements in simulating observed leads. Current metrics used to evaluate ice model skill [Prellar and Posey, 1996; Van Woert et al., 2001, 2004] are an adaptation of a least squares metric [e.g., Willmott et al., 1985] adopted from operational numerical weather prediction data assimilation systems. These systems score a forecast skill based

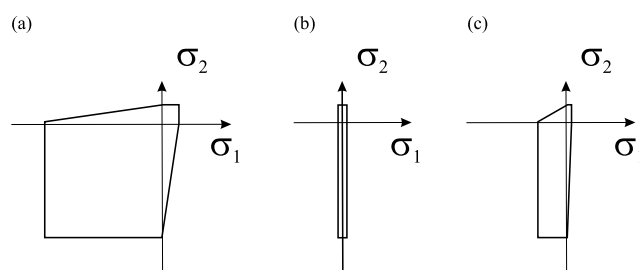


Figure 11. Failure surface for pack ice (a) with no leads, (b) with a new lead, and (c) with a partially refrozen lead.

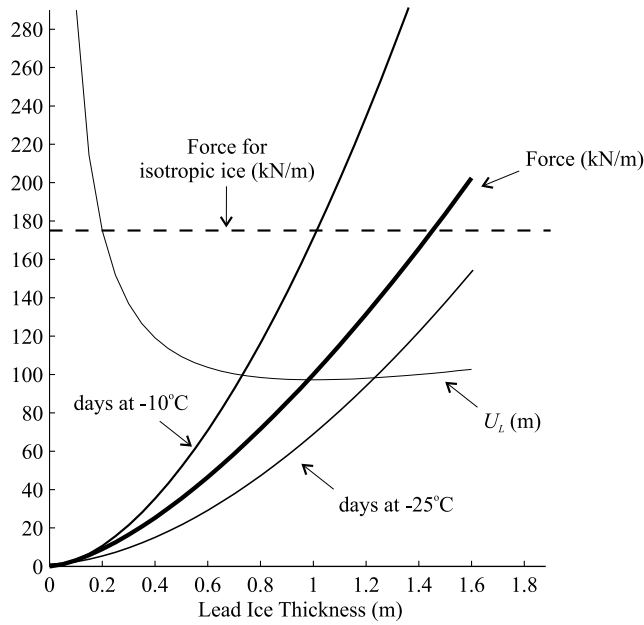


Figure 12. Limit ridging force and the lead width required to reach the limit ridging force vary as a function of the lead ice thickness. Days required to grow lead ice to different thickness is shown for two examples. The compression force required to fail isotropic ice is obtained from Figure 8.

on the standard error of a model value summed over all grid points and normalized by the difference from either climatology or persistence. These metrics are most appropriate for continuous fields and Eulerian systems where the observations and predictions are commensurate. They have replaced correlation-based indices as measures of model accuracy. However, this class of metrics suffers from some flaws in areas of sharp gradients and discontinuities (e.g., leads) and when Lagrangian treatments are more natural. For example, when the variables are validated against non-synoptic and/or satellite observations, discrepancies in the location of linear features between model prediction/analysis and observations may result in a low skill score or in the rejection of good observations as outliers in a quality controlled system. These problems are further exacerbated in Arctic regions where linear features (leads) comprise a small yet extremely important area of the domain, and satellite observations with uncertain observational errors and inaccuracies are often the sole data source for validation. The use of common metrics in these circumstances can result in the rejection of the only data available by a quality controlled assimilation scheme when features are dislocated. Similarly, poor forecasts that fail to predict or diagnose these important features, may score much better by these metrics than forecasts which identify the dynamically important features, albeit at a somewhat different location or orientation than observations indicate.

[42] We describe two metrics specifically designed to measure model accuracy in representing linear features (e.g., leads). The indices circumvent the requirement that both the observations and model variables will be commensurate (i.e., measured with the same units) by considering the frequencies of the features of interest and importance. We illustrate the metrics by scoring several hypothetical

simulated discontinuity fields against the lead interpreted from the RGPS observation of a 50 km by 50 km region of the Arctic (shown in Figure 6). An idealized representation of the area with the simulated and RGPS discontinuity features on an undeformed mesh is shown in Figure 14.

[43] Consider L features of interest and N spatial segments of the domain. N is determined on the basis of the spatial scales considered of importance. We define our first metric, the fractional index of agreement as

$$A_f = \left(\sum_{i=1}^L w_i \sum_{j=1}^N w_j F_{ij} \right) / \left(\sum w \right), \quad (12)$$

where F_{ij} is the fractional agreement in terms of grid-cell count of the i th feature in the j th spatial segment and w are the weights given to the features and the spatial segments.

[44] We now define a second metric to evaluate model success in representing features. It, too, treats features through a frequency distribution at predetermined spatial segments of the domain. The second metric shares many of the characteristics of the fractional index of agreement, but takes the more familiar format of standard error common in routine distance or root mean square (RMS) skill indices,

$$I_A = 1 - \sqrt{\left(\sum_{i=1}^L w_i \sum_{j=1}^N w_j D_{ij} \right) / \left(\sum w \right)}, \quad (13)$$

where w are the same as for the fractional index of agreement, and $D_{i,j}$ is a normalized frequency difference or distance function: $D_{i,j} = \frac{(p_{i,j} - o_{i,j})^2}{(p_{i,j} + o_{i,j})^2}$, where $p_{i,j}$ and $o_{i,j}$ are the predicted (simulated) and observed feature frequencies (cell count) of feature i in segment j .

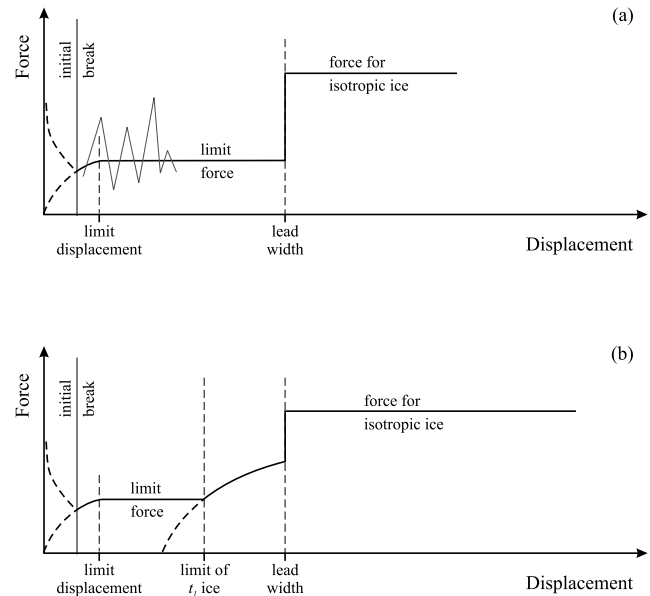
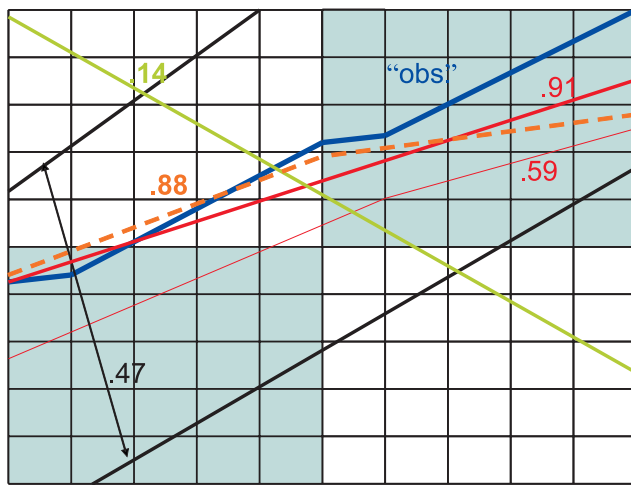
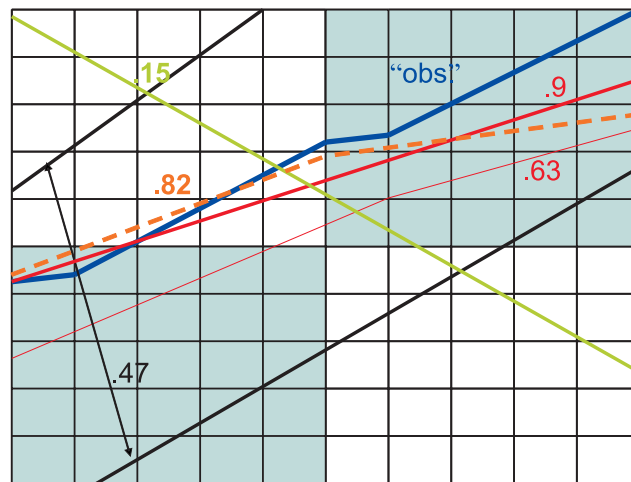


Figure 13. Force displacement curves for a lead under riding showing (a) lead with a single ice thickness and (b) lead with two thicknesses of ice where t_1 is the thinnest ice present.



(a)



(b)

Figure 14. (a) Fractional Agreement Index (A_f) and (b) Agreement Index (I_A) scores for 4 (color-coded) synthetic “simulations.” Only partial agreement in orientation is assumed in the upper right quadrant for the dashed line. The two “simulated” parallel cracks ($A_f = I_A = 0.407$) are scored together as one simulation.

[45] In the examples shown in Figure 14, we consider, using both indices, the agreement in (1) the existence of leads; and (2) the existence of leads at the observed orientation and the spatial distribution of this agreement in the entire simulated or observed domain (in this case a 50 km by 50 km region), as well as in its parts (the four shaded 25 km by 25 km quadrants). We thus score $L = 2$ features at $N = 5$ parts of the domain. The metrics are based on cell count, are nondimensional, and yield scores that range in values between 0 (no agreement) and 1 (perfect agreement). Here we assume that all weights, $w = 1$, but in the general case they could be adjusted according to the relative importance assigned or desired of a specific feature or scale, as well as for known errors or biases. For example, one could set w_i near 1 when accuracy is considered more important for some features, and w_j near 1 for deformed or

uneven grid cells or when observations and simulations are temporally or spatially separated.

[46] Figure 14 displays the location and orientation of four synthetic simulations along with their agreement scores using both agreement indices (A_f and I_A) with respect to the RGPS observed lead (marked as “obs.”) using equal weights for the two features and the five segments considered. Using the same criteria, the two indices produce remarkably consistent scores.

6. Summary and Conclusion

[47] This paper revisits the AIDJEX assumptions about pack ice behavior with an eye to modeling sea ice dynamics. The AIDJEX assumptions that (1) enough leads were present in a 100 km by 100 km region to make the ice isotropic on that scale; (2) the ice had no tensile strength; and (3) the ice behavior can be approximated by an isotropic yield surface are critically reexamined. The review of these assumptions suggests a different view of the dynamics of pack ice based on different assumptions. The new view of the behavior would lead to a model that accounts directly for velocity (displacement) discontinuities. These discontinuities are related to the formation of leads and ridges and would give rise to anisotropic ice strength. This new view is based on the detailed deformation data provided by RADARSAT and measured sea ice stress. Displacement data show that discontinuities in velocity caused by lead opening, closing, and shear must be accounted for in the representation of deformation. Ice stress data show that during lead formation the lead is traction free, and only stress parallel to the lead can be supported. The result is anisotropic behavior for pack ice with the deformation occurring on discontinuities in the displacement (or velocity) field. We have presented the kinematics relating a continuous interpretation of ice velocity data to a discontinuous interpretation. Finally, we presented a metric that would be appropriate for validation of a discontinuous model against observed displacement data. We conclude that observations of stress and ice motion do not support the assumptions common to most ice dynamic models in use today, and new models based on different assumptions are needed.

[48] **Acknowledgments.** This work was supported by Minerals Management Service and the National Aeronautics and Space Administration (under contract NNH04 CC 45C), the Office of Naval Research (under contract N000-14-04-M-0005) and the National Science Foundation (under grant DMS-0222253). We thank two anonymous reviewers and R. S. Pritchard for careful review of the paper.

References

- Coon, M. D. (1980), A review of AIDJEX modeling, in *Sea Ice Processes and Models: Symposium Proceedings 1980*, edited by R. S. Pritchard, pp. 12–27, Univ. of Wash. Press, Seattle.
- Coon, M. D., and P. A. Lau (1990), The effect of viscoelastic sea ice behavior on limited driving forces, paper presented at 1990 Offshore Technology Conference, Am. Assoc. of Pet. Geol., Richardson, Tex.
- Coon, M. D., P. A. Lau, S. H. Bailey, and B. J. Taylor (1989), Observations of ice floe stress in the eastern Arctic, paper presented at POAC '89: The 10th International Conference on Port and Ocean Engineering under Arctic Conditions, Int. Conf. on Port and Ocean Eng. Under Arctic Conditions, Luleå, Sweden.
- Coon, M. D., D. C. Eckert, and G. S. Knoke (1992), Pack ice anisotropic constitutive model, paper presented at the 11th International Symposium on Ice, Int. Assoc. for Hydraulic Res., Banff, Alberta, Canada.

- Coon, M. D., G. S. Knoke, D. C. Eckert, and R. S. Pritchard (1998a), The architecture of an anisotropic elastic-plastic sea ice mechanics constitutive law, *J. Geophys. Res.*, *103*(C10), 21,915–21,925.
- Coon, M. D., D. C. Eckert, and G. S. Knoke (1998b), Stress validation of a failure (yield) surface for pack ice, in *Ice in Surface Waters: Proceedings of the 14th International Symposium on Ice*, edited by H. T. Shen, pp. 1049–1055, Int. Glaciol. Soc., Potsdam, N. Y.
- Grumbine, R. W. (1998), Virtual floe ice drift forecast model intercomparison, *Weather Forecasting*, *13*, 886–890.
- Hibler, W. D., III (1979), A dynamic/thermodynamic sea ice model, *J. Phys. Oceanogr.*, *9*(4), 815–846.
- Hibler, W. D., III (1980), Modeling pack ice as a viscous-plastic continuum: Some preliminary results, in *Sea Ice Processes and Models: Symposium Proceedings 1980*, edited by R. S. Pritchard, pp. 163–176, Univ. of Wash. Press, Seattle.
- Hibler, W. D., III (2004), Modelling the dynamic response of sea ice, in *Mass Balance of the Cryosphere: Observations and Modeling of Contemporary and Future Changes*, edited by J. L. Bamber and A. J. Payne, pp. 227–334, Cambridge Univ. Press, New York.
- Hopkins, M. A. (1998), Four stages of pressure ridging, *J. Geophys. Res.*, *103*(C10), 21,883–21,891.
- Hunke, E. C., and J. K. Dukowicz (1997), An elastic-viscous-plastic model for sea ice dynamics, *J. Phys. Oceanogr.*, *27*(9), 1849–1867.
- Kwok, R. (2006), Contrasts in sea ice deformation and production in the Arctic seasonal and perennial ice zones, *J. Geophys. Res.*, *111*, C11S22, doi:10.1029/2005JC003246.
- Marsan, D., H. Stern, R. Lindsay, and J. Weiss (2004), Scale dependence and localization of the deformation of Arctic sea ice, *Phys. Rev. Lett.*, *93*(17), doi:10.1103/PhysRevLett.93.178501.
- Maykut, G. A. (1986), The surface heat and mass balance, in *Geophysics of Sea Ice*, edited by N. Untersteiner, pp. 395–462, Plenum Press, London.
- Parmeter, R. R., and M. D. Coon (1972), A model of pressure ridge formation in sea ice, *J. Geophys. Res.*, *77*(33), 6565–6575.
- Prellar, R. H., and P. G. Posey (1996), Validation test report for a navy sea ice forecasting system: The Polar Ice Prediction System 2.0, *Rep. NRL/FR/7322-95-9634*, Nav. Res. Lab., Stennis Space Center, Miss.
- Pritchard, R. S. (1980), A simulation of nearshore winter ice dynamics in the Beaufort Sea, in *Sea Ice Processes and Models: Symposium Proceedings 1980*, edited by R. S. Pritchard, pp. 49–61, Univ. of Wash. Press, Seattle.
- Pritchard, R. S. (1981), Mechanical behavior of pack ice, in *Mechanics of Structured Media, Part I*, edited by A. P. S. Selvadurai, pp. 371–405, Elsevier, Amsterdam.
- Pritchard, R. S. (1998), Ice conditions in an anisotropic sea ice dynamics model, *Int. J. Offshore Polar Eng.*, *8*(1), 9–15.
- Sanderson, T. J. O. (1988), *Ice Mechanics: Risks to Offshore Structures*, Graham and Trotman, London.
- Schreyer, H. L., D. L. Sulsky, L. B. Munday, M. D. Coon, and R. Kwok (2006), Elastic-decohesive constitutive model for sea ice, *J. Geophys. Res.*, *111*, C11S26, doi:10.1029/2005JC003334.
- Sulsky, D., H. Schreyer, K. Peterson, R. Kwok, and M. Coon (2007), Using the material-point method to model sea ice dynamics, *J. Geophys. Res.*, *112*, C02S90, doi:10.1029/2005JC003329.
- Thorndike, A. S., and R. Colony (1978), Estimating the Deformation of Sea Ice, *AIDJEX Bull.* *37*, pp. 25–36, Univ. of Wash., Seattle.
- Tuhkuri, J., M. Lensu, and M. A. Hopkins (1998), Laboratory and field studies on ridging of an ice sheet, in *Proceedings of the 14th International Symposium on Ice*, edited by H. T. Shen, pp. 591–602, Int. Assoc. for Hydraulic Res., Potsdam, New York.
- Van Woert, M. L., W. N. Meier, C.-Z. Zou, J. A. Beesley, and P. D. Hovey (2001), Satellite validation of the May 2000 sea ice concentration fields from the Polar Ice Prediction System, *Can. J. Remote Sens.*, *27*(5), 443–456.
- Van Woert, M. L., C.-Z. Zou, W. N. Meier, and P. D. Hovey (2004), Verification of the “Polar Ice Prediction System” sea ice concentration field, *J. Atmos. Oceanic Technol.*, *21*(6), 944–957.
- Willmott, C. J., S. G. Ackleson, R. E. Davis, J. J. Feddema, K. M. Klink, D. R. Legates, J. O’Donnell, and C. M. Rowe (1985), Statistics for the evaluation and comparison of models, *J. Geophys. Res.*, *90*(C5), 8995–9005.

M. Coon, G. Levy, and M. Pruis, NorthWest Research Associates, Redmond, WA 98052, USA. (max@nwra.com; gad@nwra.com; matt@nwra.com)

R. Kwok, Jet Propulsion Laboratory, Pasadena, CA 91109, USA. (ron.kwok@nasa.jpl.gov)

H. Schreyer, Department of Engineering, University of New Mexico, Albuquerque, NM 87131, USA. (schreyer@me.unm.edu)

D. Sulsky, Department of Mathematics and Statistics, University of New Mexico, Albuquerque, NM 87131, USA. (sulsky@math.unm.edu)